Applied Thermal Engineering 228 (2023) 120459

Contents lists available at ScienceDirect

Applied Thermal Engineering

journal homepage: www.elsevier.com/locate/apthermeng

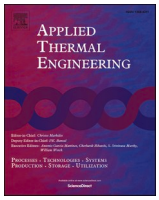

Research Paper

Thermal performance of cold thermal energy storage system with fin and fin–foam structures

Chuanqi Chen [a], Yanhua Diao [a,*], Yaohua Zhao [a,b], Zeyu Wang [a], Yifa Han [a], Zhen Wang [a], Yutong Liu [a], Dongran Fang [a], Tingting Zhu [c,d]

[a] Beijing Key Laboratory of Green Built Environment and Efficient Technology, Beijing University of Technology, Beijing 100124, China
[b] Zibo Boi Energy Science and Technology Co., Ltd., Shandong 255000, China
[c] Department of Thermal and Fluid Engineering, Faculty of Engineering Technology (ET), University of Twente, 7522 NB Enschede, the Netherlands
[d] Tianjin Key Lab of Refrigeration Technology, Tianjin University of Commerce, Tianjin 300134, China

ARTICLE INFO

Keywords:
Cold thermal energy storage
Heat transfer enhancement
Fin
Metal foam
Effectiveness

ABSTRACT

The heat transfer performance of most cold thermal energy storage (CTES) devices is limited by the low thermal conductivity of phase change materials (PCMs) and the increase in the thickness of PCMs. A comparative work was performed to explore the heat transfer performance of CTES systems with a fin structure (Fin-CTES) and a fin–foam structure (Fin–foam-CTES). The heat transfer performance, temperature distribution, and thermal effectiveness of Fin-CTES and Fin–foam-CTES at different inlet temperatures and volume flow rates of heat transfer fluid were investigated and compared. Results demonstrated that the overall heat transfer performance of Fin–foam-CTES is better than that of Fin-CTES. However, compared with the PCM in Fin-CTES, that in Fin–foam-CTES has a greater degree of supercooling, reaching 4.35 °C at the maximum. In the discharging (melting) process, Fin-CTES and Fin–foam-CTES have almost similar heat transfer effectiveness, in which the maximum difference is only 0.0107. That is, the enhanced heat transfer effect of the natural convection of the liquid PCM and the metal foam is basically the same during the discharging process.

1. Introduction

With the economic development and the rapid urbanization, the demand for and the consumption of commercial electric power have gradually increased worldwide. The peak of urban power grids is also increased in the requirements of new large buildings and building comfort. Therefore, the safety and stability of power supply are facing great challenges due to the peak–valley difference of power grids. To ensure the safety and stable operation of grids, power load adjustment is crucial [1,2].

Power load adjustment includes the supply-side adjustment of the means of expanding/adjusting power generation equipment and the demand-side adjustment of the means of transferring/adjusting electricity time. Given that the former is restricted by investment and fossil energy consumption/pollution, the latter has received increasing attention gradually [3]. As the main source of peak commercial power consumption, the operating load for air conditioning accounts for 20%–40% of the commercial electricity load; thus, adjusting the air conditioning time is beneficial to load shifting [4,5]. Load shifting with a diurnal cool storage system is the technology of storing the cold of night and releasing the cold energy during the day, and it is an effective means of weakening the peak of power [6].

As an important part of load shifting with a diurnal cool storage system, a cold thermal energy storage (CTES) system with high heat transfer efficiency ensures the high efficiency of the system [7]. Water is widely used as a phase change material (PCM) for cold storage due to its advantages of low cost, easy availability, and large latent heat of phase change. Researchers have developed various ice cold storage devices, including coil type [8,9], encapsulation type [10], sleeve type [11], tube bundle type [12], and heat pipe type [13], to meet the needs of cold storage air conditioners.

However, the challenge in the above structure is that the heat transfer rate gradually decreases with the increase in the thickness of the ice layer, and the evaporation temperature of the refrigerator will also decrease [14]. The methods of extending the heat exchange area [15,16], optimizing the structure [17,18], and utilizing composite PCMs [19,20] have been adopted to solve this problem. Jannesari [15] used experiments and simulation methods to study the influence of the structural parameters of two CTES systems with annular fins or rings on

* Corresponding author.
E-mail address: diaoyanhua@bjut.edu.cn (Y. Diao).

https://doi.org/10.1016/j.applthermaleng.2023.120459
Received 18 June 2022; Received in revised form 28 January 2023; Accepted 21 March 2023
Available online 24 March 2023

Nomenclature

CTES	Cold thermal energy storage
HTF	Heat transfer fluid
PCM	Phase change material

Dimensional variables

c_p	Specific heat capacity (J/kg·°C)
H	Latent heat (J/kg)
Re	Reynolds number
t	Time (s)
T	Temperature (°C)
Ste	Stefan number
x	Independent variable of equipment
y	Experimental result
ε	Effectiveness
$\bar{\varepsilon}$	Average effectiveness

Subscripts

in	Inlet
i / n	Number of independent variables
pcm	Phase change material
out	Outlet
u	Supercooling

ice solidification rate. The results showed that compared with a bare tube, the annular fins and rings could increase the solidification rate of ice by 21% and 34%, respectively. Zheng [16] established a numerical model of concentric tube CTES and studied the effects of different pipe diameters and materials on the ice melting and solidification behavior. The results indicated that increasing the tube diameter could accelerate the heat transfer rate of ice, but increasing the thermal conductivity of the tube would not significantly improve the heat transfer rate. Kayansayan [17] used experimental and numerical simulation methods to study the effects of different structural parameters of a fin tube, including fin spacing and size, on the melting and solidification rates of ice. The results showed that compared with the energy storage rate of a bare tube, that of a fin tube with a fin density of 31 fins/m and a dimensionless diameter of 3.2 was increased by more than 45%. Hamzeh [18] established a two-dimensional ice-on-coil numerical model and studied the influences of fin structural parameters, fin number, and tube arrangement on the thermal performance of CTES. The author found that the number and height of fins were the main factors affecting the thermal performance. Yang [19] used experiments and numerical simulation methods to study the solidification behavior of a composite PCM of copper foam–water at different porosities and pore densities. The results showed that the porosity of the foam was the dominant factor affecting the thermal performance of CTES. To study the influence of metal foam contact conditions on the thermal performance of CTES, Feng [20] tested the solidification performance of composite PCMs of foamed copper–water under three contact conditions: natural contact, pressure contact, and high-thermal-conductivity silicone bonding. The results showed that the CTES had a similar solidification rate under the above three contact conditions. However, Feng [20] ignored the effect of contact conditions on PCM supercooling and only considered the effect on ice growth.

The methods of using fins to expand the heat transfer area and using foam–water composite PCM are two common ways to enhance the heat transfer rate of CTES. Comparison of these two methods shows that metal fins, which are characterized by high thermal penetration, can transmit heat through PCM rapidly but cannot improve the heat diffusion rate of PCM. The unique structure of metal foams with high porosity and high specific surface area is conducive to the heat diffusion of PCM, but the thermal penetration is relatively weak. A new structure that combines fin and metal foam should be developed, given that this structure may have the advantages of the fin and metal foam. In [21], Fang used an experimental method to study the solidification characteristics of ice in a CTES system with a fin–foam structure. The author considered the impact of the structural parameters of fin size and number on the performance of CTES with fin–foam. The results showed that the solidification rate of ice could be accelerated when a fin was inserted into the metal foam. Fins would strengthen the natural convection of liquid PCM, whereas metal foams would inhibit that [22]. However, Fang only studied/compared the heat transfer performance of CTES systems with a pure foam copper structure and a fin–foam structure. The heat transfer performance of CTES systems with a fin–foam structure and a pure fin structure was not evaluated in the comparative study, and only the solidification (charging) process was studied by the author. Whether the heat transfer performance of a CTES system with a fin–foam structure is better than that of a CTES system with a pure fin structure is worth exploring.

For filling the abovementioned research gaps, this study established two CTES systems with straight fins (Fin-CTES) and with fin–foam (Fin–foam-CTES) as enhanced heat transfer measures. The heat transfer performance, temperature distribution, and thermal effectiveness of Fin-CTES and Fin–foam-CTES were investigated and compared. The main contributions of this study are as follows:

1. A metal foam and straight fin coupled heat transfer structure was used to accelerate the output of cold energy.

2. The heat transfer performance of Fin-CTES and Fin–foam-CTES in the charging and discharging processes was compared, which provided a reference for the design of related CTES.

This research first elucidated the experimental device. Then, the charging and discharging performance of Fin-CTES and Fin–foam-CTES at different inlet temperatures and volume flow rates of heat transfer fluid (HTF) was experimentally studied. Lastly, effectiveness was used to evaluate/compare the heat transfer performance of Fin-CTES and Fin–foam-CTES structures.

2. Experimental setup and procedure

2.1. Experimental setup

The schemes for the experimental setup are shown in Figs. 1, 2, and 3. Both devices had a multichannel flat tube with tiny fins as HTF channels. A glycol–water solution with a volume concentration of 30% was used as HTF. Distilled water was used as PCM and encapsulated into the gap of fins or foamed metal with polycarbonate plates. The difference between the two devices was that one used straight fins to enhance the heat transfer on the ice side (Fin-CTES), whereas the other added foam iron in the fin gap (Fin–foam-CTES). To reduce the contact thermal resistance, thermal silica with thermal conductivity of 1.2 W/(m·K) was used to attach straight fins to the surface of the multichannel flat tube. In Fin–foam-CTES, a natural contact existed between the foam iron and the straight fins, and no adhesive was used. To make the heat exchange performance of Fin-CTES and Fin–foam-CTES comparable, the same mass (2.6 kg) of distilled water was filled into the two devices. In consideration of the volume expansion of PCM during solidification, the filling rates for liquid PCM of the two devices were 89% and 92%. The actual volume ratio of metal in the iron foam was 1.58% (the ratio of the volume of metal to the volume of the test section of CTES). The structural parameters of the multichannel flat tube, straight fin, and foam iron are shown in Table 1. The physical properties of the glycol–water solution (with 0 °C as an example) and foam iron are shown in Table 2.

2.2. Experimental system

A schematic of the experimental setup is presented in Fig. 4. The system mainly consisted of three parts:

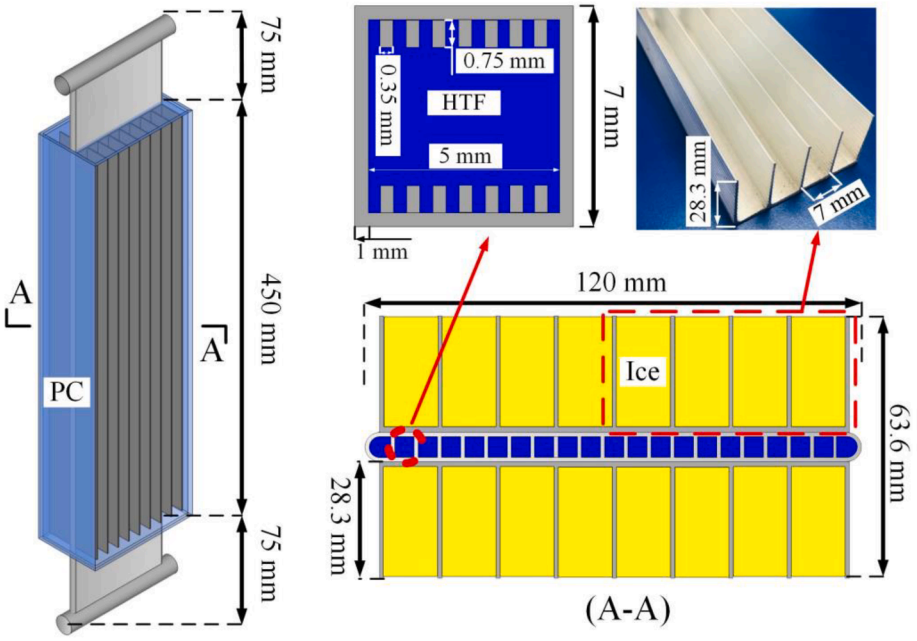

Fig. 1. Structure of Fin-CTES.

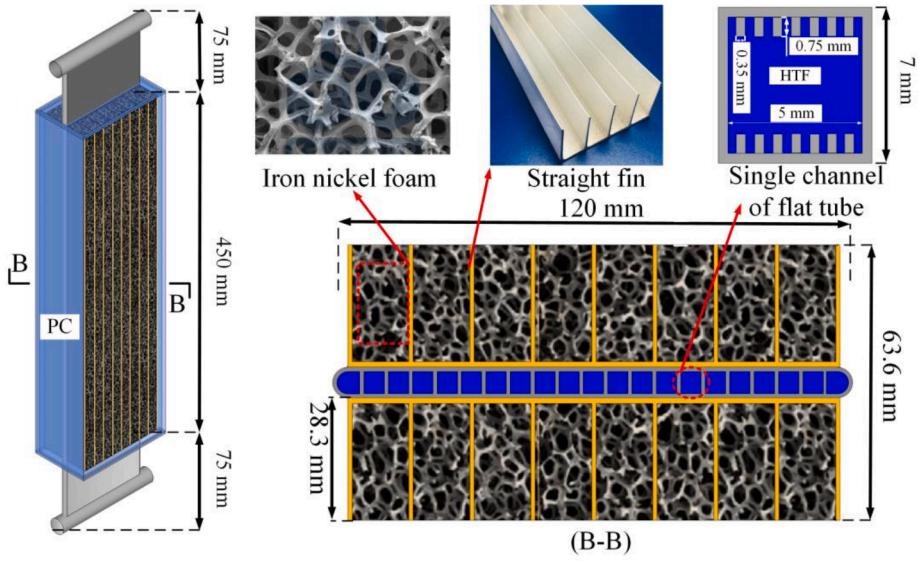

Fig. 2. Structure of Fin–foam-CTES.

(1) The tested device, Fin-CEST or Fin–foam-CEST, was wrapped in insulation cotton to reduce heat loss.
(2) The HTF circulation system mainly included a low-temperature ethylene glycol bath, a valve, a flowmeter, and a PVC pipeline. The ethylene glycol bath served as a cold/heat source (−10 °C–90 °C) and provided the circulating power for HTF at the same time.
(3) The data acquisition system was composed of resistance thermometers, a data collector, and a computer.

The experiment was mainly divided into two processes: cold storage and cold release. The solidification process of PCM was the filling of cold energy, hereinafter referred to as "charging." On the contrary, the melting process of PCM was the release of cold energy, hereinafter referred to as "discharging". The thermal performance of the two devices under different inlet temperatures and HTF flow rates was tested and compared. Table 3 shows the accuracy and error of the measurement parameters of the experimental instrument.

Figs. 5 and 6 respectively present the positions of resistance thermometers for temperature measurement in Fin-CTES and Fin–foam-CTES. From Fig. 5, nine resistance thermometers (T101, T102, T103, T104, T105 and T106, T107, T103, T108) were evenly arranged in the length (gravity) and width (horizontal) directions of the straight fin to monitor the temperature changes of PCM. Three resistance thermometers (T109, T103, and T110) were arranged in the height direction of the straight fin. Four resistance thermometers were arranged at the inlet (T111 and T112) and outlet (T113 and T114) of the device to monitor the energy transfer of HTF. The arrangement of resistance thermometers in Fin–foam-CTES was similar, but the number started with T3-.

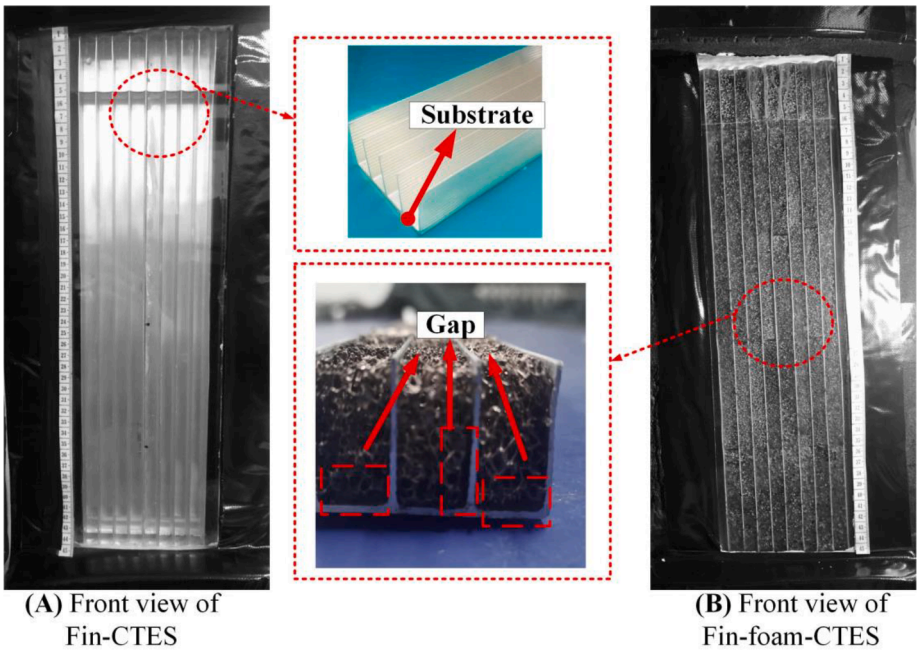

Fig. 3. Setup images of Fin-CTES and Fin–foam-CTES.

Table 1
Structural parameters of the multichannel flat tube, straight fin, and foam iron.

Parameters	Value
Straight fin pitch	7 mm
Straight fin thickness	1 mm
Straight fin size (length × width × height)	450 mm × 110 mm × 28.3 mm
Multichannel flat tube size (length × width × height)	600 mm × 120 mm × 7 mm
Single channel size (length × width × height)	450 mm × 5 mm × 5 mm
Number of flat tube channels	21
Foam iron porosity	96%
Foam iron PPI	8
Foam iron size (length × width × height)	450 mm × 6 mm × 26 mm

Table 2
Physical properties of the glycol–water solution (with 0 °C as an example), fin, and foam iron.

Physical properties	Value
Thermal conductivity of iron foam	43.2 W/(m·K)
Density of iron foam	7790 kg/m^3
Specific heat capacity of iron foam	470 J/(kg·K)
Thermal conductivity of fin	162 W/(m·K)
Density of fin	2660 kg/m^3
Specific heat capacity of fin	871 J/(kg·K)
Thermal conductivity of glycol–water solution	0.429 W/(m·K)
Density of glycol–water solution	1051.78 kg/m^3
Specific heat capacity of glycol–water solution	3890 J/(kg·K)
Dynamic viscosity of glycol–water solution	0.00415 Pa·s

2.3. Error analysis

The measurement error of the experimental instruments was the cause of the relative error of the experimental data. If the data y were a function of independent variables x_1, x_2, x_3, …, x_n, then

$$y = x_1^{a_1} x_2^{a_2} x_3^{a_3} \cdots x_n^{a_n} \tag{1}$$

The relative error was defined as [23]

$$\frac{w_y}{y} = \left[\sum_{i=1}^{n} \left(\frac{a_i w_{xi}}{x_i} \right)^2 \right]^{\frac{1}{2}} \tag{2}$$

where w_y and w_{xi} are the uncertainty in y and the measurement of independent variable x_i, respectively. i and n are the numbers of independent variables. Effectiveness, a dimensionless performance parameter, was used to evaluate the heat transfer performance of CTES (Eq. (3)). With reference to Table 3 and **Eq. (2)**, the maximum relative errors of the effectiveness of Fin-CTES and Fin–foam-CTES in the charging and discharging processes were 7.81% and 5.96%, respectively.

3. Results and discussion

3.1. Temperature distribution within CTES systems

Fig. 7 presents the temperature distribution of PCM in the gravity direction in Fin-CTES and Fin–foam-CTES during the charging process. The inlet temperature and flow rate of HTF of both devices are − 5 °C and 1 L/min, respectively, and the initial temperature of the two devices is the same at 5 °C.

From Fig. 7, the solidification process can be divided into three stages: sensible heat stage (stage 1), subcooling stage (stage 2), and solidification stage (stage 3). The sensible heat stage is when the liquid water drops from 5 °C to 0 °C. The supercooling stage is further divided into nucleation and grain growth stages. The solidification stage is mainly the formation and spread of solid ice. The temperature of the PCM in both devices is basically consistent before 75 min. After 75 min, the liquid PCM in CTES gradually completes the solidification process in the order from the bottom to the top. The temperature distribution in CTES does not change significantly in the charging (solidification) process after a metal foam is added. The straight fins, which are characterized by high thermal penetration, dominate the heat transfer on the PCM side in both devices. However, the supercooling degree of PCM (T_u) near T301 in Fin–foam-CTES is significantly higher than that in Fin-CTES, reaching 4.35 °C. In Fin-CTES and Fin-foam-CTES, solid ice is first produced on the fin wall and substrate surface. The difference is that in Fin-foam-CTES, metal foam promotes the rapid transfer of heat

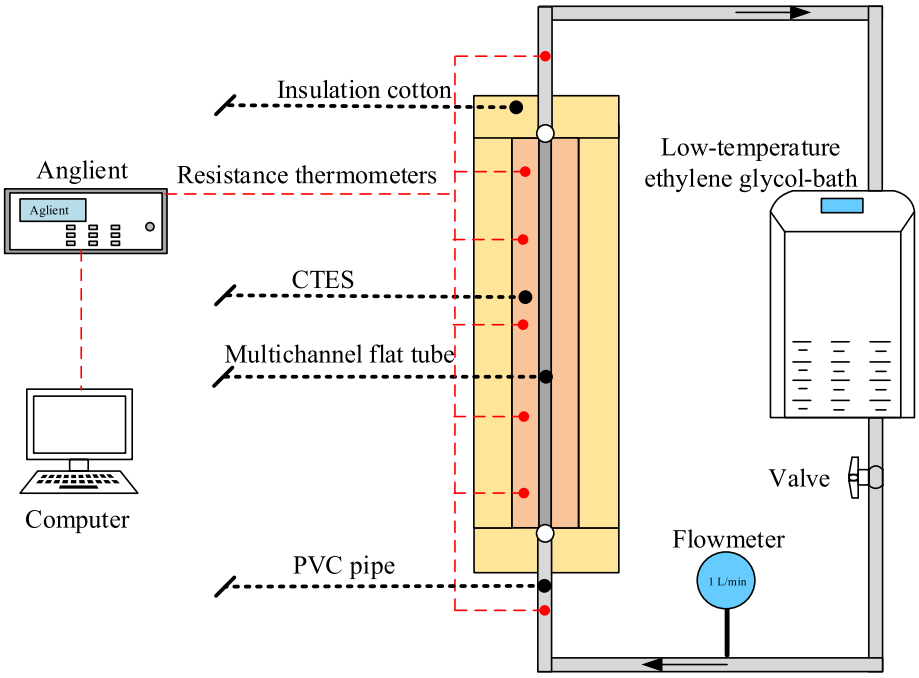

Fig. 4. Schematic of the experimental system.

Table 3
Accuracy/error of the instruments used in the experiment.

Name	Model	Range	Accuracy
Ethylene glycol bath	DTY-20	−10 °C–90 °C	± 0.1 °C
Agilent (data collector)	34970A	–	–
Resistance thermometer	PT100	−50 °C–200 °C	± 0.2 °C
Flowmeter	LDG-10SF	0–5 L/min	± 0.2%

from liquid water that has not reached the phase transition temperature to the fin and substrate surface, causing the liquid-cooled this way to undergo a metastable state when it reaches the nominal phase transition point. Hence, it should be pointed out that all phase change occurs in metastable conditions. In the metastable region, substances cannot spontaneously change phase, they are influenced by external impurities/ structures and energy [24]. The metal foam's unique porous structure increases the metastable ice formation time. That is, the nucleation and nucleation growth of this part of the liquid will be delayed, resulting in more proactive cooling below the nominal solidification point. In Fin-CTES that without metal foam, the fin and substrate surface cannot suck heat from the liquid as fast as that in Fin-foam-CTES. Therefore, the metastable condition time emphasized above will be shorter, while the sub-cooling phenomenon will be less evident.

Fig. 8 illustrates the temperature distribution of PCM in the gravity direction in Fin-CTES and Fin–foam-CTES during the discharging process (melting). Fig. 9 shows the field maps of Fin-CTES and Fin–foam-CTES during charging and discharging. The inlet temperature and flow rate of HTF of both devices are 10 °C and 1 L/min, respectively, and the initial temperature of the two devices is the same at −5 °C. T101 and T301 indicate that the melting rate of PCM in Fin–foam-CTES is faster

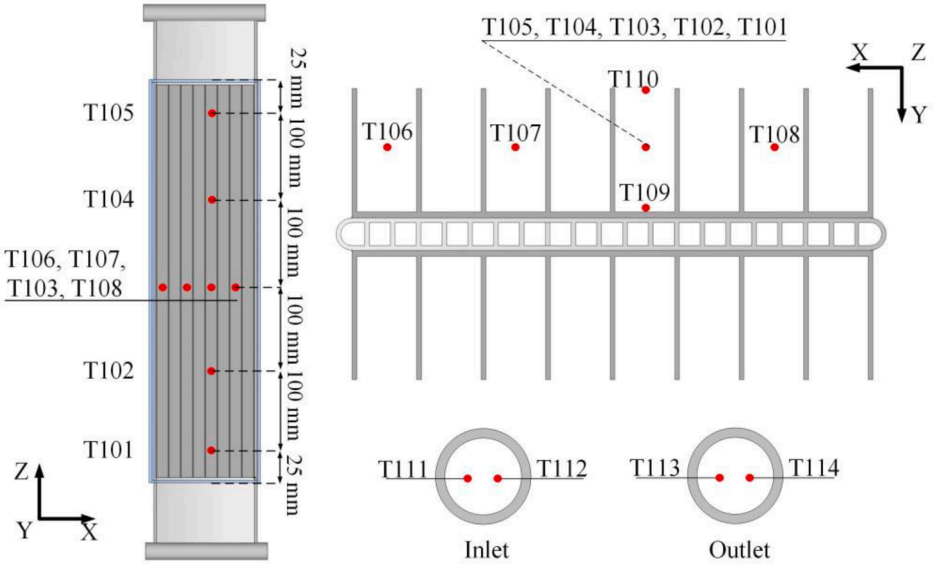

Fig. 5. Locations of resistance thermometers in Fin-CTES.

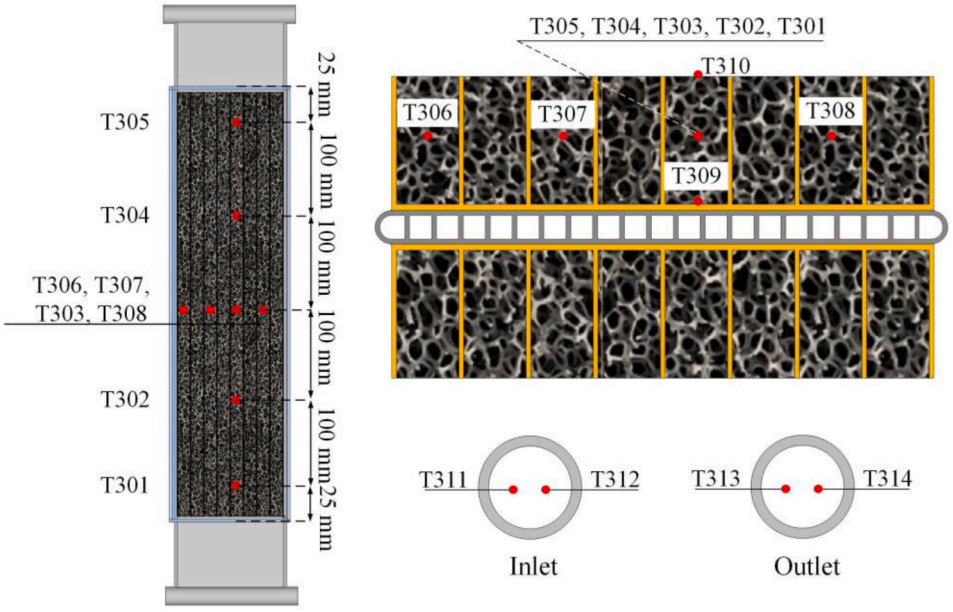

Fig. 6. Locations of resistance thermometers in Fin–foam-CTES.

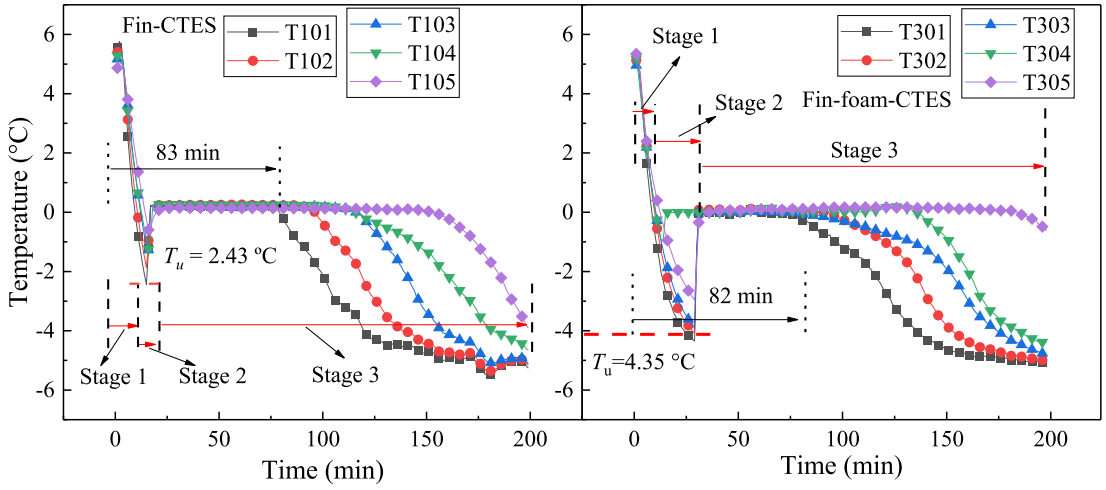

Fig. 7. Temperature distribution of Fin-CTES (left) and Fin–foam-CTES (right) during the charging process.

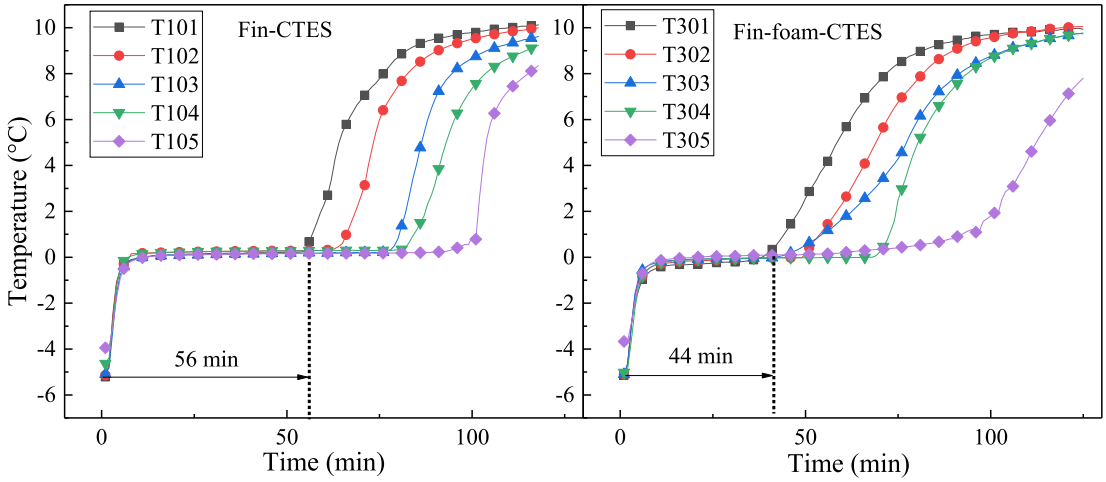

Fig. 8. Temperature distribution of Fin-CTES (left) and Fin–foam-CTES (right) during the discharging process.

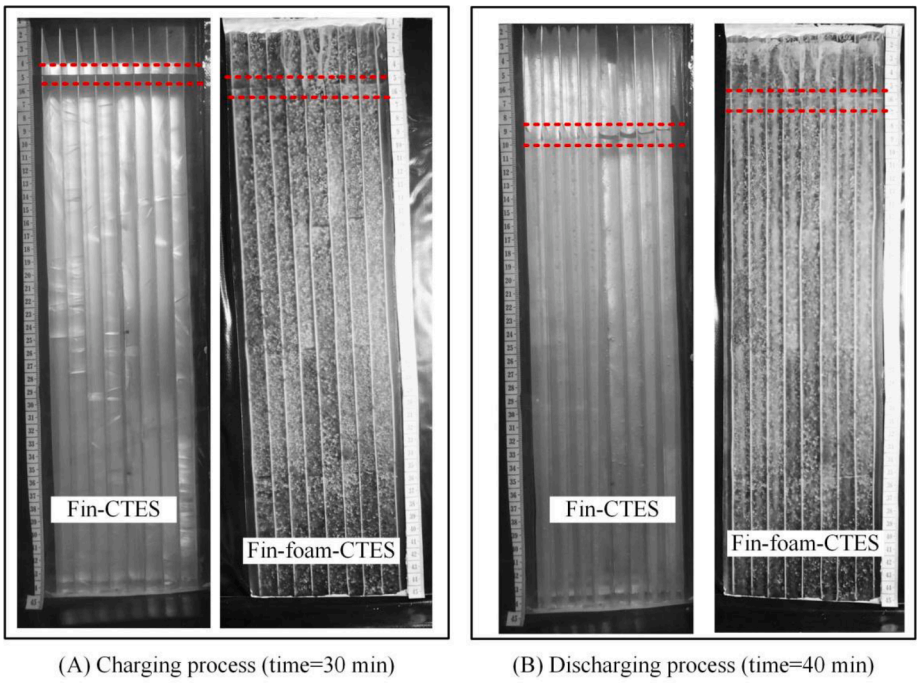

Fig. 9. Field maps of Fin-CTES and Fin–foam-CTES during charging (A) and discharging (B).

than that in Fin-CTES. Although the natural convection of liquid PCM in Fin–foam-CTES is suppressed, the higher thermal conductivity of composite PCMs will compensate for this deficiency. The temperature uniformity of the PCM inside both Fin-CTES and Fin–foam-CTES is poor. A high-temperature HTF (10 °C) is injected from the lower part of the CTES, which will inevitably lead to an increase in the temperature of the PCM in Fin-CTES and Fin–foam-CTES from bottom to top. Owing to the effect of volume shrinkage during the ice melting process, air gaps will exist in the ice layer near the T105/T305 point (Fig. 9), causing the ice melting rate here to be significantly slow. As shown in Fig. 9, the gas–liquid interface is located between the two dashed lines.

3.2. *Effect of inlet temperature on the CTES performance*

Fig. 10 illustrates the temperature of PCM at the central point in Fin-CTES (T103) and Fin–foam-CTES (T303) during the charging process at different inlet temperatures (−3 °C, −4 °C, −5 °C, −6 °C, and −7 °C). The initial temperature and flow rate of HTF of both devices are 5 °C and 1 L/min, respectively. From Fig. 10, the effect of inlet temperature on the heat exchange performance of the two devices is evident, even if there is only an increment of 1 °C. For Fin-CTES, the inlet temperature is reduced from − 3 °C to −7 °C, and the time to complete solidification of the T103 point is reduced from 237 min to 88 min, indicating a reduction of approximately 78%. The reduction in inlet temperature speeds up the solidification rate of PCM from two aspects: reducing the supercooling degree and increasing the cooling rate. For Fin–foam-CTES, the supercooling degree of the PCM is greater than 3 °C. Thus, the PCM cannot start the phase change when the inlet temperature is −3 °C, and it maintains the state of supercooling. In particular, when the inlet temperature drops from −4 °C to −7 °C, the phase change completion time of the PCM at the T303 point is inconsiderably different, all at approximately t = 66 min. The temperature drop rate of ice only accelerates with inlet temperature drop. Comparison of the supercooling degree of PCM at different inlet temperatures in the two sets of experimental data shows that inlet temperature (or cooling rate) is an important factor that affects the supercooling degree. The higher the

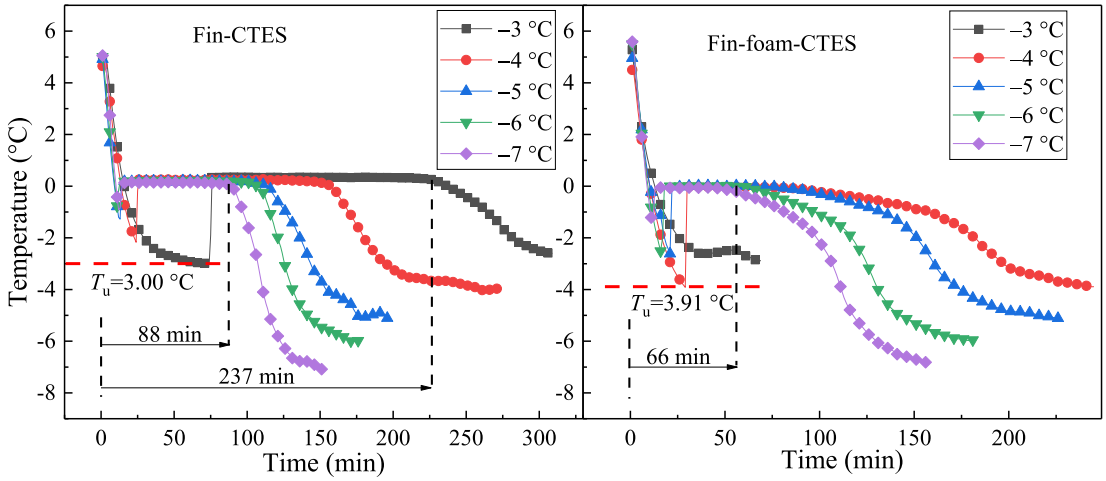

Fig. 10. Temperature curves of PCM in Fin-CTES (left) and Fin–foam-CTES (right) at different inlet temperatures during the charging process.

cooling temperature is, the lower the supercooling degree of the PCM will be.

Fig. 11 shows the temperature of PCM at the central point in Fin-CTES (T103) and Fin–foam-CTES (T303) during the discharging process at different inlet temperatures (8 °C, 9 °C, 10 °C, 11 °C, and 22 °C). The initial temperature and flow rate of HTF of both devices are −5 °C and 1 L/min, respectively. From the figure, the effect of inlet temperature on the melting rate of PCM is evident, even if the temperature change value is only 1 °C. For Fin-CTES, when the inlet temperature drops from 12 °C to 9 °C, the melting time of PCM near T103 is increased from 58 min to 90 min, i.e., by 55%. For Fin–foam-CTES, the impact of inlet temperature on the melting process is mainly focused on the temperature rise stage of PCM. This phenomenon is different from the influence of the inlet temperature of Fin-CTES. The natural convection of liquid PCM is suppressed in Fin–foam-CTES, but the heat transfer is enhanced by increasing the thermal conductivity of PCM. During the melting stage, heat can be rapidly conducted inside Fin–foam-CTES while keeping the internal temperature uniform. During the temperature rise stage of liquid water, due to the relatively low thermal conductivity of water (the effective thermal conductivity of composite PCMs is also reduced), the temperature uniformity in Fin–foam-CTES becomes poor, which shows that it is highly sensitive to the change in inlet temperature.

3.3. Effect of HTF flow rate on the CTES performance

Fig. 12 demonstrates the temperature of PCM at the central point in Fin-CTES (T103) and Fin–foam-CTES (T303) during the charging process at different volume flow rates of 0.75, 1.00, 1.25, 1.50, 1.75, and 2.00 L/min. The Reynolds numbers corresponding to a single channel are 209, 273, 337, 401, 465, and 529. The initial temperature and inlet temperature of HTF of both devices are 5 °C and −5 °C, respectively. Volume flow rate is an ignored factor affecting the thermal performance of CTES. The volume flow rate of HTF increases from 0.75 L/min to 2.00 L/min, and the time to complete solidification of PCM in Fin-CTES and Fin–foam-CTES is reduced by 65 min (42.5%) and 78 min (65.0%), respectively. For Fin-CTES, the improvement in the solidification rate of PCM is not linear as the flow rate increases. When the flow increases to 1.5 L/min, the influence of flow rate on its thermal transfer performance basically disappears. On this basis, the heat resistance of Fin-CTES is mainly concentrated on the PCM side at this time. Hence, when the heat exchange performance of the HTF side is increased, the solidification rate of PCM no longer changes significantly. On the contrary, this phenomenon does not appear in Fin–foam-CTES. The flow rate of HTF still affects the heat exchange performance of Fin–foam-CTES. After the addition of metal foam, the effective thermal conductivity of the composite PCM is indeed improved.

Fig. 13 demonstrates the temperature of PCM at the central point in Fin-CTES (T103) and Fin–foam-CTES (T303) during the discharging process at different volume flow rates of 0.75, 1.00, 1.25, 1.50, 1.75, and 2.00 L/min. The initial temperature and inlet temperature of HTF of both devices are −5 °C and 10 °C, respectively. The comparison in Fig. 12 depicts that the effect of volume flows rates on the heat transfer performance of Fin-CTES is continuous between 0.75 and 2 L/min. Increasing the volume flow rate of HTF will reduce the thermal resistance on the side of the multichannel flat tube. At the same time, the overall heat transfer thermal resistance of CTES will also decrease. Relevant studies have shown that the main heat transfer resistance of CTES is mainly concentrated on the PCM side [25]. However, in Fin-CTES, the natural convection effect of liquid PCM reduces the heat transfer thermal resistance on the PCM side. This situation results in increased sensitivity of the PCM temperature to the changes in the volume flow of HTF. For Fin–foam-CTES, the volume flow rate weakly affects the speed of PCM during the phase change period (35–50 min). This phenomenon is consistent with the charging process. Overall, the heat transfer performance of Fin–foam-CTES is better than that of Fin-CTES during the discharging process under similar conditions.

3.4. Thermal performance evaluation of Fin-CTES and Fin–foam-CTES

To compare the heat transfer performance of Fin-CTES and Fin–foam-CTES further, the dimensionless performance parameter effectiveness (ε), which represents the ratio of the actual heat exchange to the theoretical maximum heat exchange amount, is used to represent the heat transfer performance of both devices [26,27]. The instantaneous and average ε are as follows:

$$\varepsilon = \frac{T_{\text{in}} - T_{out}}{T_{in} - T_{pcm}} \tag{3}$$

$$\overline{\varepsilon} = \frac{1}{\Delta t}\int_{t_{begin}}^{t_{end}} \varepsilon dt \tag{4}$$

where T_{in}, T_{out}, and T_{pcm} are the inlet temperature of HTF, the outlet temperature of HTF, and the phase change temperature of PCM (0 °C), respectively. $\Delta t = t_{end} - t_{begin}$, where t_{end} and t_{begin} are the start and end times of the phase transition of PCM, respectively. The Stefan number is a dimensionless parameter, which not only represents the energy density of the energy storage system but also reflects the heat transfer driving force (i.e., temperature difference) of the system [28,29]. It is composed of latent heat (H), specific heat (c_p), and heat exchange temperature difference ($T_{in} - T_{pcm}$):

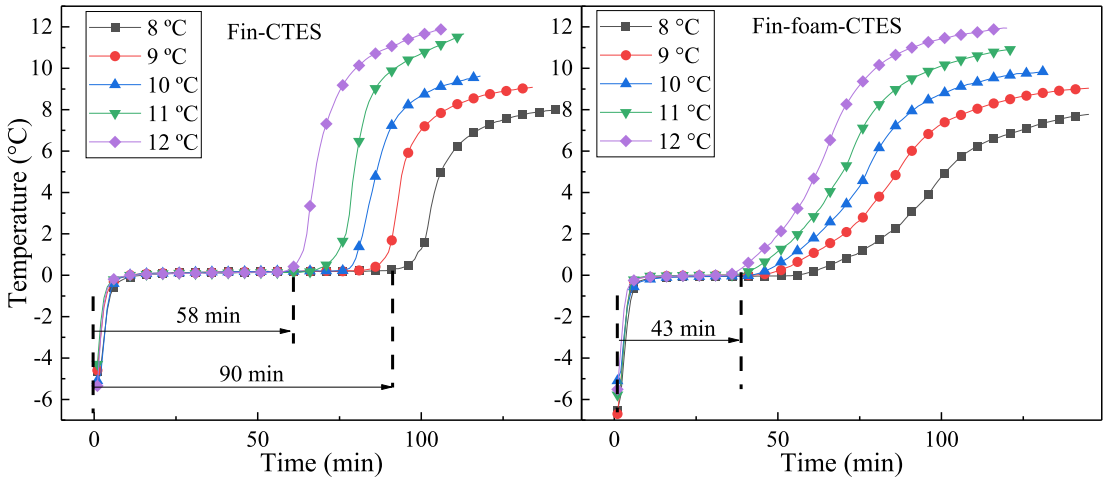

Fig. 11. Temperature curves of PCM in Fin-CTES (left) and Fin–foam-CTES (right) at different inlet temperatures during the discharging process.

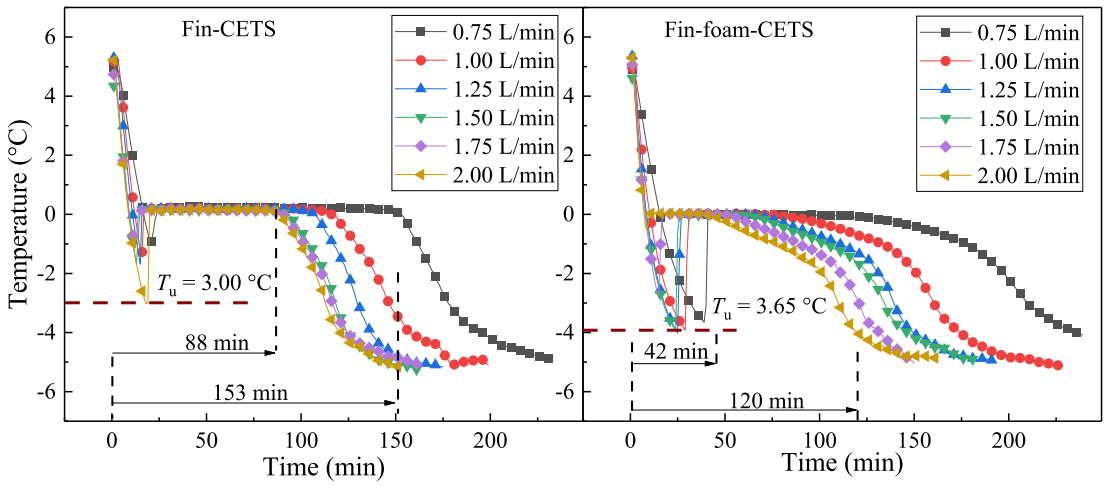

Fig. 12. Temperature curves of PCM in Fin-CTES (left) and Fin–foam-CTES (right) at different volume flow rates during the charging process.

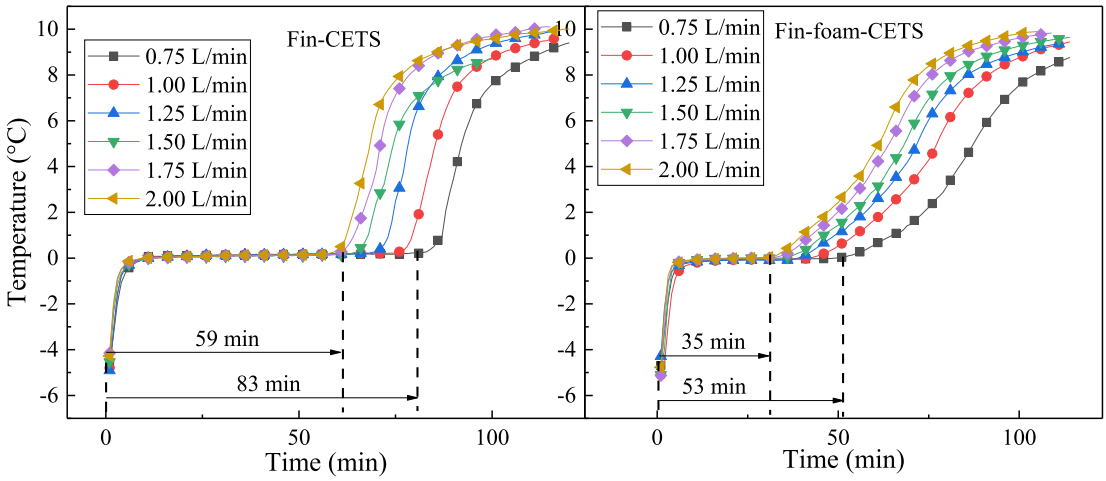

Fig. 13. Temperature curves of PCM in Fin-CTES (left) and Fin–foam-CTES (right) at different volume flow rates during the discharging process.

$$Ste = \frac{c_p|T_{in} - T_{pcm}|}{H} \quad (5)$$

Fig. 14 shows the variation in average effectiveness of Fin-CTES and Fin–foam-CTES with *Ste* in the charging process (left) and discharging process (right) and Re = 273 (constant). The data do not include the supercooling period of PCM but only represent the phase change heat transfer process. In consideration of the phenomenon of supercooling discussed earlier, a control variable is needed here. The average effectiveness gradually decreases as the number of *Ste* increases. Given T_{pcm}

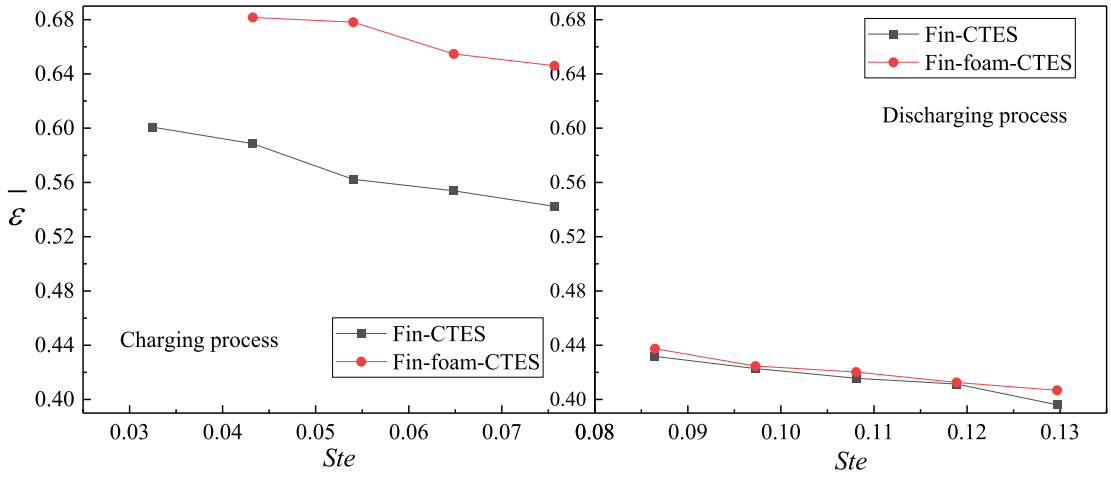

Fig. 14. Average effectiveness of Fin-CTES and Fin–foam-CTES at different *Ste* during the charging process (left) and discharging process (right), *Re* = 273.

= 0, Eq. (3) is simplified to $\varepsilon = (T_{in} - T_{out})/T_{in}$. The curve of Fin-CTES during charging is regarded as an example. When *Ste* increases from 0.043 to 0.076 (T_{in} decreases from −4 °C to −7 °C), the cooling loss of the device per unit time increases gradually, resulting in that $T_{in} - T_{out}$ does not change linearly with the linear change in T_{in}. This condition results in a gradual decrease in the effectiveness value as *Ste* (or T_{in}) increases. However, the scope of this reduction is small at the range of 0–0.05. The addition of a metal foam undoubtedly enhances the heat transfer performance of CTES in the charging and discharging processes. In particular, adding a metal foam can improve the average effectiveness with a maximum increase of 0.1159 (approximately 20.62%) during the solidification period. Nevertheless, compared with the situation in the charging process, the effectiveness of Fin-CTES and Fin–foam-CTES is considerably close in the discharging process, with a maximum difference of only 0.0107 (approximately 2.70%). During charging, the natural convection of PCM in Fin-CTES is relatively weaker than that during discharging [25], while the effective thermal conductivity of PCM in Fin–foam-CTES increases (even though the natural convection of PCM is also weak). This phenomenon enables Fin–foam-CTES to have a higher heat transfer rate, which thus leads to a large difference in the effectiveness of Fin-CTES and Fin–foam-CTES during charging. However, in the discharging process, the two respectively rely on natural convection and increase the thermal conductivity of PCM to enhance the heat transfer. This condition results in almost equal effectiveness of Fin-CTES and Fin–foam-CTES during discharging.

Fig. 15 presents the variation curves of the average effectiveness of Fin-CTES and Fin–foam-CTES at different Reynolds numbers during charging and discharging processes. These values are obtained from the phase transition period. Comparison of Figs. 14 and 15 indicates that the effectiveness of CTES decreases with the increase in *Ste* and *Re*. This phenomenon can be explained from a thermodynamic point of view. Exergy efficiency is defined as the ratio of available energy to input energy, and its physical meaning is similar to effectiveness. Bi [30] performed an exergy analysis of a CTES and found that with the increase in the difference between the HTF temperature and the phase transition temperature of PCM, the ratio of the available energy of CTES decreased. Bejan [31] studied the effect of different flow rates on the second law efficiency of an energy storage device and concluded that with the increase in flow rate (*Re*), the second law efficiency or exergy efficiency of the device decreased. Therefore, the effectiveness of CTES decreases with the increase in *Ste* and *Re*. The effect of adding a metal foam on the charging process is greater than that on the discharging process because the heat exchange temperature difference in the charging process is smaller than that in the discharging process. The addition of a metal foam can indeed increase the heat transfer rate of CTES, especially during the solidification period. However, in consideration of the high cost and high subcooling degree of Fin–foam-CTES, even if supercooling can be improved using other methods, the Fin–foam structure may not be a perfect choice for the discharging process.

4. Conclusion

To evaluate the effects of a pure fin structure and a fin–foam structure on the heat transfer performance of CTES, two devices, Fin-CTES and Fin–foam-CTES, were built in this study. The charging and discharging performance of the two devices at different inlet temperatures and volume flow rates was experimentally studied. Lastly, the heat transfer performance of the two devices was evaluated. The main conclusions are as follows:

1. Compared with the temperature distribution in Fin-CTES, that in Fin–foam-CTES is insignificantly improved. On the contrary, the maximum supercooling degree of PCM in Fin–foam-CTES reaches 4.35 °C, which indicates an increase of 1.92 °C compared with that in Fin-CTES.

2. Increasing the heat exchange temperature difference between the inlet temperature of HTF and the melting point of PCM can significantly improve the heat exchange rate of CTES even if the temperature increase is only 1 °C. When the inlet temperature is increased from −7 °C (9 °C) to −3 °C (12 °C), the solidification (melting) time of PCMs in Fin-CTES decreases by 78% (55%). In Fin–foam-CTES, the influence of inlet temperature on heat transfer is mainly concentrated in the temperature drop (rise) period during the charging (discharging) process. In addition, the higher the inlet temperature (low cooling rate) is, the greater the supercooling degree of PCM is.

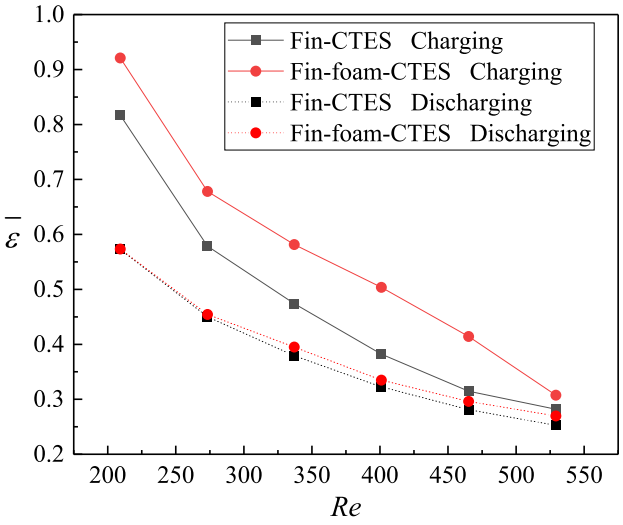

Fig. 15. Average effectiveness of Fin-CTES and Fin–foam-CTES at different Reynolds numbers during charging and discharging processes; *Ste* = 0.05404 for the charging process, and *Ste* = 0.10808 for the discharging process.

3. Compared with Fin-CTES, Fin–foam-CTES is more sensitive to the changes in HTF volume flow rate. The volume flow rate of HTF increases from 0.75 L/min to 2.00 L/min, while the time to complete solidification (melting) of PCM in Fin-CTES and Fin–foam-CTES is reduced by 42.5% (28.9%) and 65.0% (34.0%), respectively, during the charging (discharging) process.

4. The improvement in the heat transfer performance of CTES via a fin–foam structure is mainly concentrated in the solidification process and has a minimal effect on the melting process. Compared with the thermal effectiveness of Fin-CTES, that of Fin–foam-CTES is increased by 0.1159 (approximately 20.62%) in the charging process. However, given that the pure fin structure is more conducive to the natural convection of liquid PCM, the heat transfer effectiveness of Fin-CTES and Fin–foam-CTES is basically the same, with a difference of only 0.0107.

Declaration of Competing Interest

The authors declare that they have no known competing financial interests or personal relationships that could have appeared to influence the work reported in this paper.

Data availability

Data will be made available on request.

Acknowledgements

The authors gratefully acknowledge the financial support provided by Beijing Municipal Natural Science Foundation (Grant No.3192009) and the National Natural Science Foundation of China (Grant No.51906177).

References

[1] H. Selvnes, Y. Allouche, A. Hafner, Experimental characterisation of a cold thermal energy storage unit with a pillow-plate heat exchanger design, Appl. Therm. Eng. 199 (2021), 117507.

[2] R. Singh, M. Mochizuki, K. Mashiko, T. Nguyen, Heat pipe based cold energy storage systems for datacenter energy conservation, Energy 36 (2011) 2802–2811.

[3] P. Yang, C. Ji, P. Li, Y.u. Li, Z. Zhao, B. Zhang, L. Lai, Hierarchical multiple time scales cyber-physical modeling of demand-side resources in future electricity market, Int. J. Electtric. Power Energy Syat. 133 (2021), 107184.

[4] A. Mammodi, M. Robinson, Numerical analysis of heat transfer processes in a low-cost, high performance ice storage device for residential applications, Appl. Therm. Eng. 128 (2018) 453–463.

[5] J.R. Turnpenny, D.W. Etheridge, D.A. Reay, Novel ventilation cooling system for reducing air condition in buildings. part 1: testing and theoretical modelling, Appl. Therm. Eng. 20 (2000) 1019–1037.

[6] H.E. Abdelrahman, H.A. Refaey, A. Alotaibi, A.A. Abdel-Aziz, M.F. Abd Rabbo, Experimental investigations on the thermal performance of an ice storage system using twin concentric helical coil, Appl. Therm. Eng. 179 (2020), 115737.

[7] B. Zalba, J.M. Marín, L.F. Cabeza, H. Meshling, Review on thermal energy storage with phase change: materials, heat transfer analysis and applications, Appl. Therm. Eng. 23 (2003) 251–283.

[8] B.T. Jaime, A.L. Navarro, J.M. Corberán, J.C. Esteban-Matías, L. Klinkner, J. Payá, Experimental analysis of a paraffin-based cold storage tank, Int. J. Refrig. 36 (2013) 1632–1640.

[9] K. Han, J. Ji, J. Cai, Y. Gao, M.d. Feng Zhang, M. Uddin, Z. Song, Experimental and numerical investigation on a novel photovoltaic direct-driven ice storage air-conditioning system, Renew. Energy 172 (2021) 514–528.

[10] X. Jia, X. Zhai, X. Cheng, Thermal performance analysis and optimization of a spherical PCM capsule with pin-fins for cold storage, Appl. Therm. Eng. 148 (2019) 929–938.

[11] M. Caliano, N. Bianco, G. Graditi, L. Mongibello, Analysis of a phase change material-based unit and of an aluminum foam/phase change material composite-based unit for cold thermal energy storage by numerical simulation, Appl. Energy 256 (2019), 113921.

[12] Y.H. Yau, B. Rismanci, A review on cool thermal storage technologies and operating strategies, Renew. Sustain. Energy Rev. 16 (2016) 787–797.

[13] S. Tian, Q. Yang, N.a. Hui, H. Bai, S. Shao, S. Liu, Discharging process and performance of a portable cold thermal energy storage panel driven by embedded heat pipes, Energy 205 (2020), 117987.

[14] D. Maderić, Z. Čarija, B. Pavković, B. Delač, Experimental and numerical study on water ice forming on pipe columns in a limited-volume storage, Appl. Therm. Eng. 194 (2021), 117080.

[15] H. Jannesari, N. Abdollahi, Experimental and numerical study of thin ring and annular fin effects on improving the ice formation in ice-on-coil thermal storage systems, Appl. Energy 189 (2017) 369–384.

[16] Z.H. Zheng, C. Ji, W.X. Wang, Numerical simulation of internal melt ice-on-coil thermal storage system, Energy Procedia 12 (2011) 1042–1048.

[17] N. Kayansayan, M.A. Acar, Ice formation around a finned-tube heat exchanger for cold thermal energy storage, Int. J. Therm. Sci. 45 (2006) 405–418.

[18] H.A. Hamzeh, M. Miansari, Numerical study of tube arrangement and fin effects on improving the ice formation in ice-on-coil thermal storage systems, Int. Commun. Heat Mass Transf. 113 (2020), 104520.

[19] Xiaohu Yang, Qingsong Bai, Qunli Zhang, Wenju Hu, Liwen Jin, JinyueYan. Thermal and economic analysis of charging and discharging characteristics of composite phase change materials for cold storage. Applied Energy 2018; 225: 585–599.

[20] S. Feng, Y.e. Zhang, M. Shi, T. Wen, L.u. Tianjian, Unidirectional freezing of phase change materials saturated in open-cell metal foams, Appl. Therm. Eng. 88 (2015) 315–321.

[21] X. Yang, Z. Niu, Q. Bai, H. Li, X. Gui, Y. He, Experimental study on the solidification process of fluid saturated in fin foam composites for cold storage, Appl. Therm. Eng. 161 (2019), 114163.

[22] M.J. Allen, T.L. Bergman, A. Faghri, N. Sharifi, Robust heat transfer enhancement during melting and solidification of a phase change material using a combined heat pipe-metal foam or foil configuration, J. Heat Transf.: Trans. ASME 137 (2015), 102301.

[23] EA-4/02. Expression of the uncertainty of measurement in calibration. European Co-Operation for Accreditation; 1999.

[24] D. Shi, Fundamental of Materials Science, China Machine Press, China, 1999, pp. 187–192.

[25] C. Chen, Y. Diao, Y. Zhao, Z. Wang, T. Wang, L. Liang, Y. Zhang, Numerical investigation of the optimization of phase change thermal storage units with air as heat transfer fluid, J. Storage Mater. 37 (2021), 102422.

[26] N.H.S Tay, M. Belusko, F. Bruno F. An-effectiveness-NTU technique for characterizing tube-in-tank phase change thermal energy storage system. Applied Energy 2012; 91(1):309-319.

[27] C.Q. Chen, Y.H. Diao, Y.H. Zhao, W.H. Ji, Z.Y. Wang, L. Liang, Thermal performance of a thermal-storage unit by using a multichannel flat tube and rectangular fins, Appl. Energy 250 (2019) 1280–1291.

[28] W. Ye, D. Zhu, N. Wang, Numerical simulation on phase-change thermal storage/release in a plate-fin unit, Appl. Therm. Eng. 31 (2011) 3871–3884.

[29] R. Qi, Z. Wang, J. Ren, W.u. Yuling, Numerical investigation on heat transfer characteristics during melting of lauric acid in a slender rectangular cavity with flow boundary condition, Int. J. Heat Mass Transf. 157 (2020), 119927.

[30] Y. Bi, X. Liu, M. Jiang, Exergy analysis of a gas-hydrate cool storage system, Energy 73 (2014) 908–915.

[31] R. Domański, G. Fellah, Exergy analysis for the evaluation of a thermal storage system employing PCMS with different melting temperatures, Appl. Therm. Eng. 16 (1996) 907–919.